2024 European Control Conference (ECC)
June 25-28, 2024. Stockholm, Sweden

Round Trip Time based UAV State Estimation

Sholeh Yasini and Torbjörn Wigren

Abstract— **A new method for UAV state estimation based on high accuracy multi Round Trip Time measurements with respect to multiple 5G base stations is presented. The proposed algorithm employs interacting multiple model filtering, with the nonlinear measurement equations handled by extended Kalman filters. A hovering movement mode is introduced, and used together with the normal flight modes such as straight line motion and maneuvering. This approach enhances the state estimation for monitoring UAV traffic using cellular connectivity, particularly in applications such as border surveillance and safeguarding sensitive areas like airports. Simulations are used to illustrate the performance of the algorithm.**

I. Introduction

Unmanned Aerial Vehicles (UAVs), commonly referred to as drones have evolved in recent years. UAVs are today used in a variety of applications including gathering of information, disaster management, geographical mapping of inaccessible terrain, and for search and rescue operations [1]. Modern drones have high maximum speeds and extended flight endurance. By exploiting cellular connectivity they can therefore travel long distances, far beyond visual range [2]. Such new remote flight modes increase the risk for the general public. In addition, uncoordinated flight increases the risk of in-air collisions [3].

The unauthorized operation of so called rogue drones in proximity to airports poses a potential hazard to commercial aircraft. In 2018 such an incident occurred at Gatwick International Airport, London, UK, resulting in the temporary suspension of the air traffic with multi-million dollar consequences. It is also well known that UAVs are used for illegal surveillance and drug trafficking close to and across border regions. The need for wide area Air Traffic Control (ATC) for drones is therefore widely discussed in e.g. [3]-[8].

An ATC system for UAVs is complicated. UAV tracking functionality using data from cellular systems, as discussed by this paper, has several advantages. As compared to primary radar, the identity of the cellular based radio measurement is always available. This avoids the need for data association, track initiation and clutter suppression that are main tasks in a radar tracking system [9], [10]. In the present paper new Round Trip Time (RTT) measurements [11], [12], with respect to multiple 5G base stations is the main source of information. It can be noted that such measurements cannot be disabled by the drone pilot, which means that the drone tracking cannot be affected by a rogue pilot that exploits cellular connectivity for flight. Another alternative is to base the tracking on measurements of Doppler frequencies, or to use a combination of RTT and Doppler [13].

Sholeh Yasini is with DNEW NSV BB Analytics, Ericsson AB, SE-16480, Stockholm, Sweden and Torbjörn Wigren is with DNEW NSV BB RRM KI1, Ericsson AB, SE-16480, Stockholm, Sweden, sholeh.yasini,torbjorn.wigren@ericsson.com.

Several state estimators for air vehicles have been proposed in the literature. The Interacting Multiple Model (IMM) algorithm, [14]-[16], uses a Markov model to merge an arbitrary number of movement modes, typically formualted as dynamic state space models. In [17], particle filters have been proposed for enhancing air target tracking, However, it should be highlighted that particle filters, in contrast to IMM filters, are more complex and require a better measurement accuracy to deliver a significant performance improvement. There are also state estimators more simple than the IMM filter. For example, the Markov mode probabilty model can be replaced by an ad-hoc maneuvre detector [10]. However, the complexity advantage is small, at the same time as a dual mode IMM filter has been shown to give a performance comparable to ad-hoc algorithms with 10 times as many modes [13]-[16].

The main engineering contributions of the paper includes range measurement based UAV state estimation using RTT measurements from multiple 5G base stations to an UAV. The state estimation is performed in Cartesian 3D position, velocity and acceleration state coordinates of the UAV. More advanced state estimation, like estimation of the attitude of the UAV, is infeasible based on RTT ranging measurement. The data fusion is performed by three Extended Kalman Filters (EKFs) [9], that handle the nonlinear RTT measurement models, within a three mode IMM framework [14]-[16]. Technically, the movement mode includes an unconventional hovering mode, a constant velocity flight mode and a maneuver flight mode. The proposed state estimation technology also restricts direct switching between constant velocity movement and hovering. The state and measurement modeling exploits continuous time models that are sampled, which allows for processing of irregular measurements. This is a key feature for the application since the tracking system performs data fusion of RTT measurements from multiple, non-colocated base stations. This relaxes the real time requirements significantly. Note that for a fair and easy comparison of the results, the same notation as in [13] is used.

The rest of the paper is organized as follows. Section II-A defines the IMM and extended Kalman filters. The UAV movement models, measurement models, mode switch models and mode mixing for different dimension states are presented in Sections II-B, II-C, II-D and II-E. Numerical examples are given in Section III. Conclusions appear in Section IV.

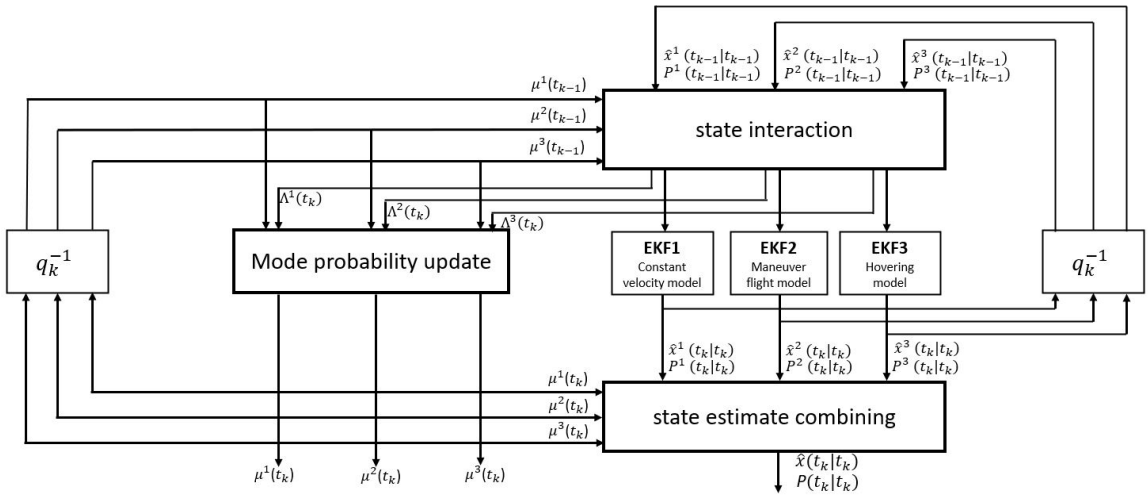

Fig. 1. Block diagram of the IMM filter depicted for three movement models of the UAV.

II. UAV State Estimation

A. IMM and Extended Kalman Filters

The IMM algorithm assumes that the system behaves according to one of a finite number of models which represents one of several movement modes. The transition model probability from one model to another model is governed by the Markovian process. Fig. 1 shows the block diagram of the IMM filter for UAV state estimation. At each time step t_k, the state estimate $\hat{\mathbf{x}}^j(t_k|t_k)$ and state covariance matrix $\hat{\mathbf{P}}^j(t_k|t_k)$ are computed under each possible model using three filters, with each filter using a different combination of the state estimates at the previous update time, as initial values.

The IMM algorithm is summarized below, cf. [9], [16]:

Step 1: Calculation of mixing probabilities. The mixing probabilities $\mu(.)$ are defined as the probability of mode j being in effect at time t_k, given that mode i was in effect at time t_{k-1}, conditioned on the data $Z^{(k-1)}$ up to time t_{k-1}. Thus

$$\mu_{i|j}(t_{k-1}|t_{k-1}) = \frac{1}{\bar{c}^j} p_{ij}(t_k, t_{k-1})\mu_i(t_{k-1}), \quad (1)$$

where p_{ij} is the transition model probability from model i to model j where $i, j = 1, 2, 3$. The normalizing constant $\bar{c}_j$ is

$$\bar{c}^j = \sum_{i=1}^{r} p_{ij}(t_k, t_{k-1})\mu_i(t_{k-1}). \quad (2)$$

The mixed initial state and covariance are obtained as

$$\hat{\mathbf{x}}^{oj}(t_{k-1}|t_{k-1}) = \sum_{i=1}^{r} \mu_{i|j}(t_{k-1}|t_{k-1})\hat{\mathbf{x}}^i(t_{k-1}|t_{k-1}), \quad (3)$$

$$\mathbf{P}^{oj}(t_{k-1}|t_{k-1}) = \sum_{i=1}^{r} \mu_{i|j}(t_{k-1}|t_{k-1}) \left(\mathbf{P}^i(t_{k-1}|t_{k-1}) + (\hat{\mathbf{x}}^i(t_{k-1}|t_{k-1}) - \hat{\mathbf{x}}^{oj}(t_{k-1}|t_{k-1})) \times (\hat{\mathbf{x}}^i(t_{k-1}|t_{k-1}) - \hat{\mathbf{x}}^{oj}(t_{k-1}|t_{k-1}))^T\right). \quad (4)$$

Here $\times$ denotes multiplication.

Step 2: The mode-conditioned filtering is performed by three EKFs. Each mode is modeled as a linear stochastic difference equation, obtained by sampling from a stochastic differential equation, and a nonlinear measurement equation. Since the measurement update requires a linearized measurement matrix in case the EKF is used [9], the linearization of the measurement equation around the predicted state is needed.

The underlying stochastic difference equation of the EKF is

$$\mathbf{x}^j(t_{k+1}) = \mathbf{A}^j(t_{k+1}, t_k)\mathbf{x}^j(t_k) + \mathbf{w}^j(t_k) \quad (5)$$

$$z^j(t_k) = h^j(\mathbf{x}^j(t_k)) + e^j(t_k), \quad (6)$$

where $\mathbf{x}(t_k)$ is the system state, $\mathbf{A}^j(t_{k+1}, t_k)$ is the system matrix, and $z^j(t_k)$ is the measurement model. The process noise is denoted by $\mathbf{w}^j(t_k)$, while $e^j(t_k)$ denotes the measurement noise. The corresponding covariance matrix and variance are denoted $\mathbf{Q}^j(t_k, t_{k-1})$ and $R^j(t_k)$.

This results in the EKF iteration

$$\hat{\mathbf{x}}^j(t_k|t_{k-1}) = \mathbf{A}^j(t_k, t_{k-1})\hat{\mathbf{x}}^j(t_{k-1}|t_{k-1})$$

$$\mathbf{P}^j(t_k, t_{k-1}) = \mathbf{A}^j(t_k, t_{k-1})\mathbf{P}^j(t_{k-1}|t_{k-1}) \times \left(\mathbf{A}^j(t_k, t_{k-1})\right)^T + \mathbf{Q}^j(t_k, t_{k-1})$$

$$\hat{z}^j(t_k|t_{k-1}) = h^j(\hat{\mathbf{x}}^j(t_k|t_{k-1}))$$

$$\mathbf{H}^j(\hat{\mathbf{x}}^j(t_k|t_{k-1})) = \frac{\partial h^j(\hat{\mathbf{x}})}{\partial \hat{\mathbf{x}}}_{|\hat{x}=\hat{x}^j(t_k|t_{k-1})}$$

$$\varepsilon^j(t_k) = z^j(t_k) - \hat{z}^j(t_k|t_{k-1})$$

$$S^j(t_k) = \mathbf{H}^j(\hat{\mathbf{x}}^j(t_k|t_{k-1}))\mathbf{P}^j(t_k|t_{k-1})$$

$$\times \left(\mathbf{H}^j(\hat{\mathbf{x}}^j(t_k|t_{k-1}))\right)^T + R^j(t_k)$$

$$\mathbf{K}^j(t_k) = \frac{1}{S^j(t_k)}\mathbf{P}^j(t_k|t_{k-1})\left(\mathbf{H}^j(\hat{\mathbf{x}}^j(t_k|t_{k-1}))\right)^T$$

$$\hat{\mathbf{x}}^j(t_k|t_k) = \hat{\mathbf{x}}^j(t_k|t_{k-1}) + \mathbf{K}^j(t_k)\varepsilon^j(t_k)$$

$$\mathbf{P}^j(t_k|t_k)$$

$$= \mathbf{P}^j(t_k|t_{k-1}) - \frac{1}{S^j(t_k)}\mathbf{K}^j(t_k)\left(\mathbf{K}^j(t_k)\right)^T, \quad (7)$$

where $\hat{\mathbf{x}}(t_k|t_{k-1})$ is the predicted state, $\hat{z}^j(t_k|t_{k-1})$ the predicted measurement, $\varepsilon^j(t_k)$ denotes the prediction error, and $\mathbf{K}^j(t_k)$ is the Kalman gain. Note that the above EKF processes each scalar measurement separately, thereby avoiding a matrix inversion step. This is natural for the nonuniformly sampled EKF above, cf. [13].

Step 3: The mode probability evaluation requires the likelihood of the latest measurement, $z(t_k)$, conditioned on the mode and the initial state and covariance matrices, i.e.,

$$\Lambda^j(t_k) = \frac{1}{\sqrt{2\pi S^j(t_k)}} e^{-\frac{(z(t_k)-h^j(\hat{\mathbf{x}}^{oj}(t_{k-1}|t_{k-1})))^2}{2S^j(t_k)}}, \quad (8)$$

where $\Lambda^j(t_k)$ denotes the likelihood function for mode j, and $h^j(\hat{\mathbf{x}}^{oj}(t_{k-1}|t_{k-1})$ is the nonlinear measurement prediction at time t_k, given the initial state estimate. The corresponding predicted variance is given by

$$S^j(t_k) = \mathbf{H}^j(\hat{\mathbf{x}}^{oj}(t_{k-1}|t_{k-1}))\mathbf{P}^{oj}(t_{k-1}|t_{k-1})$$

$$\times \left(\mathbf{H}^j(\hat{\mathbf{x}}^{oj}(t_{k-1}|t_{k-1}))\right)^T + R^j(t_k). \quad (9)$$

The mode probabilities become

$$c = \sum_{j=1}^{r} \Lambda^j(t_k)\bar{c}^j, \quad (10)$$

$$\mu^j(t_k) = \Lambda^j(t_k)\bar{c}^j. \quad (11)$$

Step 4: At the final step, the combination of the mode state estimates and covariance matrix are obtained as

$$\hat{\mathbf{x}}(t_k|t_k) = \sum_{j=1}^{r} \mu^j(t_k)\hat{\mathbf{x}}^j(t_k|t_k), \quad (12)$$

$$\mathbf{P}(t_k|t_k) = \sum_{j=1}^{r} \mu^j(t_k)\left(\mathbf{P}^j(t_k|t_k) + (\hat{\mathbf{x}}^j(t_k|t_k) - \hat{\mathbf{x}}(t_k|t_k))\left(\hat{\mathbf{x}}^j(t_k|t_k) - \hat{\mathbf{x}}(t_k|t_k)\right)^T\right). \quad (13)$$

B. UAV Movement Models

The new combination of movement modes include constant velocity movement, constant acceleration movement and hovering constant position movement which are detailed in the following.

1) Constant velocity movement model: The states of the constant velocity movement model are

$$\mathbf{x}^1 = \begin{pmatrix} x_1^1 & x_2^1 & x_3^1 & \dot{x}_1^1 & \dot{x}_2^1 & \dot{x}_3^1 \end{pmatrix}^T. \quad (14)$$

The first three states represent the Cartesian position state variables, with the third state representing altitude, the last three state variables represent the corresponding velocity components.

The stochastic differential equation for the constant velocity model is

$$d\mathbf{x}^1(t) = \mathbf{F}^1\mathbf{x}^1(t)dt + \mathbf{G}^1 d\mathbf{w}^1(t), \quad (15)$$

where the matrix $\mathbf{F}^1$ and the matrix $\mathbf{G}^1$ are [9]

$$\mathbf{F}^1 = \begin{pmatrix} 0 & 0 & 0 & 1 & 0 & 0 \\ 0 & 0 & 0 & 0 & 1 & 0 \\ 0 & 0 & 0 & 0 & 0 & 1 \\ 0 & 0 & 0 & 0 & 0 & 0 \\ 0 & 0 & 0 & 0 & 0 & 0 \\ 0 & 0 & 0 & 0 & 0 & 0 \end{pmatrix}, \quad (16)$$

$$\mathbf{G}^1 = \begin{pmatrix} 0 & 0 & 0 \\ 0 & 0 & 0 \\ 0 & 0 & 0 \\ 1 & 0 & 0 \\ 0 & 1 & 0 \\ 0 & 0 & 1 \end{pmatrix}. \quad (17)$$

2) Constant acceleration movement model: The constant acceleration model is defined using the states

$$\mathbf{x}^2 = \begin{pmatrix} x_1^2 & x_2^2 & x_3^2 & \dot{x}_1^2 & \dot{x}_2^2 & \dot{x}_3^2 & \ddot{x}_1^2 & \ddot{x}_2^2 & \ddot{x}_3^2 \end{pmatrix}^T. \quad (18)$$

The model is:

$$d\mathbf{x}^2(t) = \mathbf{F}^2\mathbf{x}^2(t)dt + \mathbf{G}^2 d\mathbf{w}^2(t), \quad (19)$$

with

$$\mathbf{F}^2 = \begin{pmatrix} 0 & 0 & 0 & 1 & 0 & 0 & 0 & 0 & 0 \\ 0 & 0 & 0 & 0 & 1 & 0 & 0 & 0 & 0 \\ 0 & 0 & 0 & 0 & 0 & 1 & 0 & 0 & 0 \\ 0 & 0 & 0 & 0 & 0 & 0 & 1 & 0 & 0 \\ 0 & 0 & 0 & 0 & 0 & 0 & 0 & 1 & 0 \\ 0 & 0 & 0 & 0 & 0 & 0 & 0 & 0 & 1 \\ 0 & 0 & 0 & 0 & 0 & 0 & 0 & 0 & 0 \\ 0 & 0 & 0 & 0 & 0 & 0 & 0 & 0 & 0 \\ 0 & 0 & 0 & 0 & 0 & 0 & 0 & 0 & 0 \end{pmatrix}, \quad (20)$$

$$\mathbf{G}^2 = \begin{pmatrix} 0 & 0 & 0 \\ 0 & 0 & 0 \\ 0 & 0 & 0 \\ 0 & 0 & 0 \\ 0 & 0 & 0 \\ 0 & 0 & 0 \\ 1 & 0 & 0 \\ 0 & 1 & 0 \\ 0 & 0 & 1 \end{pmatrix}. \quad (21)$$

3) Constant position model: The constant position hovering model is defined by the states

$$\mathbf{x}^3 = \begin{pmatrix} x_1^3 & x_2^3 & x_3^3 \end{pmatrix}^T. \quad (22)$$

The model is:

$$d\mathbf{x}^3(t) = \mathbf{F}^3\mathbf{x}^3(t)dt + \mathbf{G}^3 d\mathbf{w}^3(t), \quad (23)$$

where

$$\mathbf{F}^3 = \begin{pmatrix} 0 & 0 & 0 \\ 0 & 0 & 0 \\ 0 & 0 & 0 \end{pmatrix}, \mathbf{G}^3 = \begin{pmatrix} 1 & 0 & 0 \\ 0 & 1 & 0 \\ 0 & 0 & g \end{pmatrix}. \quad (24)$$

where parameter g in the process noise gain matrix $\mathbf{G^3}$ is set to allow for more horizontal drift than vertical drift. The process noise covariance for the three modes denoted by $\mathbf{M}^j$ is defined as

$$\mathbf{M}^j = \begin{pmatrix} q_1^j & 0 & 0 \\ 0 & q_2^j & 0 \\ 0 & 0 & q_3^j \end{pmatrix}. \quad (25)$$

The models (15), (19) and (23) need to be discretized for IMM implementation, see [9] p. 192. A stochastic sampling using $T_k = t_k - t_{k-1}$ as sampling interval, results in the following system matrices and system noise covariance matrices

$$\mathbf{A}^1(t_k, t_{k-1}) = \mathbf{A^1}(T_k) = \begin{pmatrix} 1 & 0 & 0 & T_k & 0 & 0 \\ 0 & 1 & 0 & 0 & T_k & 0 \\ 0 & 0 & 1 & 0 & 0 & T_k \\ 0 & 0 & 0 & 1 & 0 & 0 \\ 0 & 0 & 0 & 0 & 1 & 0 \\ 0 & 0 & 0 & 0 & 0 & 1 \end{pmatrix}, \quad (26)$$

$$\mathbf{A}^2(t_k, t_{k-1}) = \mathbf{A^2}(T_k) = \begin{pmatrix} 1 & 0 & 0 & T_k & 0 & 0 & 0 & 0 & 0 \\ 0 & 1 & 0 & 0 & T_k & 0 & 0 & 0 & 0 \\ 0 & 0 & 1 & 0 & 0 & T_k & 0 & 0 & 0 \\ 0 & 0 & 0 & 1 & 0 & 0 & T_k & 0 & 0 \\ 0 & 0 & 0 & 0 & 1 & 0 & 0 & T_k & 0 \\ 0 & 0 & 0 & 0 & 0 & 1 & 0 & 0 & T_k \\ 0 & 0 & 0 & 0 & 0 & 0 & 1 & 0 & 0 \\ 0 & 0 & 0 & 0 & 0 & 0 & 0 & 1 & 0 \\ 0 & 0 & 0 & 0 & 0 & 0 & 0 & 0 & 1 \end{pmatrix}, \quad (27)$$

$$\mathbf{A}^3(t_k, t_{k-1}) = \mathbf{A^3}(T_k) = \begin{pmatrix} 1 & 0 & 0 \\ 0 & 1 & 0 \\ 0 & 0 & 1 \end{pmatrix}. \quad (28)$$

$$\mathbf{Q}^1(t_k, t_{k-1}) = \mathbf{Q}^1(T_k) = \begin{pmatrix} \mathbf{Q}_1^1(T_k) & \mathbf{Q}_2^1(T_k) \\ \mathbf{Q}_2^1(T_k) & \mathbf{Q}_3^1(T_k) \end{pmatrix}, \quad (29)$$

where

$$\mathbf{Q}_1^1(T_k) = \begin{pmatrix} \frac{1}{3}q_1^1 T_k^3 & 0 & 0 \\ 0 & \frac{1}{3}q_2^1 T_k^3 & 0 \\ 0 & 0 & \frac{1}{3}q_3^1 T_k^3 \end{pmatrix}, \quad (30)$$

$$\mathbf{Q}_2^1(T_k) = \begin{pmatrix} \frac{1}{2}q_1^1 T_k^2 & 0 & 0 \\ 0 & \frac{1}{2}q_2^1 T_k^2 & 0 \\ 0 & 0 & \frac{1}{2}q_3^1 T_k^2 \end{pmatrix}, \quad (31)$$

$$\mathbf{Q}_3^1(T_k) = \begin{pmatrix} q_1^1 T_k & 0 & 0 \\ 0 & q_2^1 T_k & 0 \\ 0 & 0 & q_3^1 T_k \end{pmatrix}, \quad (32)$$

$$\mathbf{Q}^2(t_k, t_{k-1}) = \mathbf{Q}^2(T_k) = \begin{pmatrix} \mathbf{Q}_{11}^2(T_k) & \mathbf{Q}_{12}^2(T_k) & \mathbf{Q}_{13}^2(T_k) \\ \mathbf{Q}_{21}^2(T_k) & \mathbf{Q}_{22}^2(T_k) & \mathbf{Q}_{23}^2(T_k) \\ \mathbf{Q}_{31}^2(T_k) & \mathbf{Q}_{32}^2(T_k) & \mathbf{Q}_{33}^2(T_k) \end{pmatrix}, \quad (33)$$

where $\mathbf{Q}_{12}^2(T_k) = \mathbf{Q}_{21}^2(T_k)$, $\mathbf{Q}_{13}^2(T_k) = \mathbf{Q}_{31}^2(T_k)$, $\mathbf{Q}_{23}^2(T_k) = \mathbf{Q}_{31}^2(T_k)$ and

$$\mathbf{Q}_{11}^2(T_k) = \begin{pmatrix} \frac{1}{5}q_1^2 T_k^5 & 0 & 0 \\ 0 & \frac{1}{5}q_2^2 T_k^5 & 0 \\ 0 & 0 & \frac{1}{5}q_3^2 T_k^5 \end{pmatrix}, \quad (34)$$

$$\mathbf{Q}_{12}^2(T_k) = \begin{pmatrix} \frac{1}{4}q_1^2 T_k^4 & 0 & 0 \\ 0 & \frac{1}{4}q_2^2 T_k^4 & 0 \\ 0 & 0 & \frac{1}{4}q_3^2 T_k^4 \end{pmatrix}, \quad (35)$$

$$\mathbf{Q}_{13}^2(T_k) = \mathbf{Q}_{22}^2(T_k) = \begin{pmatrix} \frac{1}{3}q_1^2 T_k^3 & 0 & 0 \\ 0 & \frac{1}{3}q_2^2 T_k^3 & 0 \\ 0 & 0 & \frac{1}{3}q_3^2 T_k^3 \end{pmatrix}, \quad (36)$$

$$\mathbf{Q}_{23}^2(T_k) = \begin{pmatrix} \frac{1}{2}q_1^2 T_k^2 & 0 & 0 \\ 0 & \frac{1}{2}q_2^2 T_k^2 & 0 \\ 0 & 0 & \frac{1}{2}q_3^2 T_k^2 \end{pmatrix}, \quad (37)$$

$$\mathbf{Q}_{33}^2(T_k) = \begin{pmatrix} q_1^2 T_k & 0 & 0 \\ 0 & q_2^2 T_k & 0 \\ 0 & 0 & q_3^2 T_k \end{pmatrix}, \quad (38)$$

$$\mathbf{Q}^3(t_k, t_{k-1}) = \mathbf{Q}^3(T_k) = \begin{pmatrix} q_1^3 T_k & 0 & 0 \\ 0 & q_2^3 T_k & 0 \\ 0 & 0 & q_3^3 T_k \end{pmatrix}. \quad (39)$$

C. Nonlinear Measurement Model

One way to measure range in cellular systems is to measure the travel time of radio waves from a base station to a mobile and back, i.e. perform an RTT measurement [11], [12]. A radio frame is transmitted from the base station to the UAV transceiver. The time between reception and transmission in the UAV, denoted T_{RxTx}, is recorded by the UAV transceiver, and reported to the base station. The base station computes the two way radio time of flight as

$$z_{RTT}(t_k) = T_{RTT} = t_{Rx} - t_{Tx} - T_{RxTx}. \tag{40}$$

where t_{Tx} and t_{Rx} are transmission time and reception time of the base station. In case of a Line-of-Sight (LOS) transmission, the measurement can now be modeled in terms of the states of the UAV and the speed of light c, which results in

$$z^j(t_k) = \frac{2}{c} d^j(\hat{\mathbf{x}}(t_k|t_{k-1})) + e_{RTT}(t_k), \tag{41}$$

$$R^j(t_k) = E[e_{RTT}(t_k)]^2. \tag{42}$$

$$d^j(\hat{\mathbf{x}}(t_k|t_{k-1})) = \Bigg(\left(\hat{x}_1^j(t_k|t_{k-1}) - x_1^s\right)^2 + \left(\hat{x}_2^j(t_k|t_{k-1}) - x_2^s\right)^2 + \left(\hat{x}_3^j(t_k|t_{k-1}) - x_3^s\right)^2 \Bigg)^{\frac{1}{2}}, \tag{43}$$

where the superscript ^{s} is a site number index. The measurement equation is

$$h^j(\hat{\mathbf{x}}^j(t_k|t_{k-1})) = \frac{2}{c} d^j(\hat{\mathbf{x}}(t_k|t_{k-1})). \tag{44}$$

Straightforward differentiation of (44) for the three movement modes gives

$$\frac{\partial h^1(\hat{\mathbf{x}}^1)}{\partial \hat{x}_i^1}_{|\hat{\mathbf{x}}^1 = \hat{\mathbf{x}}^1(t_k|t_{k-1})} = \begin{pmatrix} \frac{\partial h^1(\hat{\mathbf{x}}^1)}{\partial \hat{x}_1^1} & \frac{\partial h^1(\hat{\mathbf{x}}^1)}{\partial \hat{x}_2^1} & \frac{\partial h^1(\hat{\mathbf{x}}^1)}{\partial \hat{x}_3^1} & 0 & 0 & 0 \end{pmatrix}^T, \tag{45}$$

$$\frac{\partial h^1(\hat{\mathbf{x}}^1)}{\partial \hat{x}_i^1}_{|\hat{\mathbf{x}}^1 = \hat{\mathbf{x}}^1(t_k|t_{k-1})} = \frac{2}{c} \frac{\left(\hat{x}_i^1(t_k|t_{k-1}) - x_i^s\right)}{d^1(\hat{\mathbf{x}}(t_k|t_{k-1}))}, i = 1, 2, 3, \tag{46}$$

$$\frac{\partial h^1(\hat{\mathbf{x}}^1)}{\partial \hat{x}_i^1} = 0, i = 4, 5, 6. \tag{47}$$

$$\frac{\partial h^2(\hat{\mathbf{x}}^2)}{\partial \hat{x}_i^2}_{|\hat{\mathbf{x}}^2 = \hat{\mathbf{x}}^2(t_k|t_{k-1})} = \begin{pmatrix} \frac{\partial h^2(\hat{\mathbf{x}}^2)}{\partial \hat{x}_1^2} & \frac{\partial h^2(\hat{\mathbf{x}}^2)}{\partial \hat{x}_2^2} & \frac{\partial h^2(\hat{\mathbf{x}}^2)}{\partial \hat{x}_3^2} & 0 & 0 & 0 & 0 & 0 & 0 \end{pmatrix}^T, \tag{48}$$

$$\frac{\partial h^2(\hat{\mathbf{x}}^2)}{\partial \hat{x}_i^1}_{|\hat{\mathbf{x}}^2 = \hat{\mathbf{x}}^2(t_k|t_{k-1})} = \frac{2}{c} \frac{\left(\hat{x}_i^2(t_k|t_{k-1}) - x_i^s\right)}{d^2(\hat{\mathbf{x}}(t_k|t_{k-1}))}, i = 1, 2, 3, \tag{49}$$

$$\frac{\partial h^2(\hat{\mathbf{x}}^2)}{\partial \hat{x}_i^2}_{|\hat{\mathbf{x}}^2 = \hat{\mathbf{x}}^2(t_k|t_{k-1})} = 0, i = 4, ..., 9. \tag{50}$$

$$\frac{\partial h^3(\hat{\mathbf{x}}^3)}{\partial \hat{x}_i^3}_{|\hat{\mathbf{x}}^3 = \hat{\mathbf{x}}^3(t_k|t_{k-1})} = \begin{pmatrix} \frac{\partial h^3(\hat{\mathbf{x}}^3)}{\partial \hat{x}_1^3} & \frac{\partial h^3(\hat{\mathbf{x}}^3)}{\partial \hat{x}_2^3} & \frac{\partial h^3(\hat{\mathbf{x}}^3)}{\partial \hat{x}_3^3} \end{pmatrix}^T, \tag{51}$$

$$\frac{\partial h^3(\hat{\mathbf{x}}^3)}{\partial \hat{x}_i^3}_{|\hat{\mathbf{x}}^3 = \hat{\mathbf{x}}^3(t_k|t_{k-1})} = \frac{2}{c} \frac{\left(\hat{x}_i^3(t_k|t_{k-1}) - x_i^s\right)}{d^3(\hat{\mathbf{x}}(t_k|t_{k-1}))}, i = 1, 2, 3. \tag{52}$$

D. Mode Switching Model

The mode transition probability matrix of the IMM filter in (1) is selected as

$$p_{ij} = \begin{pmatrix} p_{11} & p_{12} & p_{13} \\ p_{21} & p_{22} & p_{23} \\ p_{31} & p_{32} & p_{33} \end{pmatrix}. \tag{53}$$

A new restricting transition probability model is used, related to the physics of the UAV movement. When the UAV is in constant velocity movement, an immediate stop is not possible. This means that the sequence of mode transitions is from the straight line movement mode, over the maneuver flight mode, to the hovering mode. The direct mode transmission from the first mode to the third mode is therefore forbidden. This is reflected by new constraints in the mode transition probability matrix (52) as

$$p_{13} \leq \epsilon_{13}, p_{31} \leq \epsilon_{31}, \tag{54}$$

where ϵ_{13} and ϵ_{31} are both much smaller than 1.

E. Mode Mixing for Different Dimension States

Since the state vectors of the three movement models have different dimensions, the mode mixing of the state and corresponding covariance matrix cannot be done in the standard way. A simple approach is to augment the constant velocity movement mode and constant position movement mode state vectors and covariances to match the dimension of the state vector and covariance matrix in the constant acceleration movement model, cf. [18]. Therefore, the augmented first and third mode state estimate vectors become

$$\hat{\mathbf{x}}^{(1,a)} = \begin{pmatrix} \hat{x}_1^1 & \hat{x}_2^1 & \hat{x}_3^1 & \hat{x}_4^1 & \hat{x}_5^1 & \hat{x}_6^1 & 0 & 0 & 0 \end{pmatrix}^T, \tag{55}$$

$$\hat{\mathbf{x}}^{(3,a)} = \begin{pmatrix} \hat{x}_1^3 & \hat{x}_2^3 & \hat{x}_3^3 & 0 & 0 & 0 & 0 & 0 & 0 \end{pmatrix}^T. \tag{56}$$

The corresponding augmented covariance matrices become

$$\mathbf{P}^{(j,a)}(t_k|t_k) = \begin{pmatrix} \mathbf{P}^j(t_k|t_k) & \mathbf{0} \\ \mathbf{0} & \mathbf{0} \end{pmatrix}, \tag{57}$$

where $j = 1, 3$. The augmented zeros in (57) are selected to match the dimension of the covariance of the constant acceleration movement model.

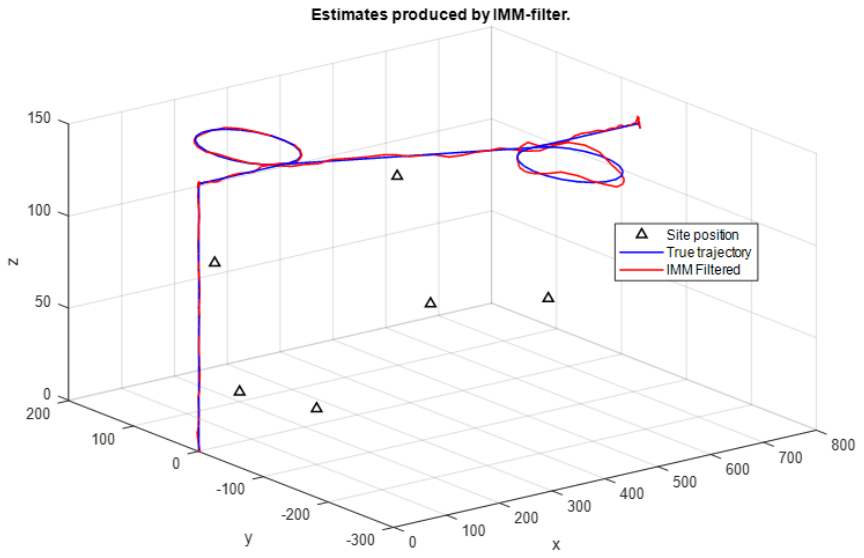

Fig. 2. Estimated drone trajectory (red) and true trajectory (blue).

III. Numerical Results

The operation and performance of the UAV state estimation algorithm are illustrated in this section. The UAV movement profile was selected to obtain a mix of three modes over time. It starts with an initial position $(\hat{x}_1(t_0|t_{-1})\ \hat{x}_2(t_0|t_{-1})\ \hat{x}_3(t_0|t_{-1}))^T = (0\ 0\ 0)^T m$ and initial velocity $(\hat{x}_4(t_0|t_{-1})\ \hat{x}_5(t_0|t_{-1})\ \hat{x}_6(t_0|t_{-1}))^T = (0\ 0\ 0)^T\ m/s$. The UAV movement profile includes constant acceleration (increasing velocity), coordinated turns (to the left and right), decreasing velocity and hovering. The base stations locations are selected as:

$$\begin{aligned} s_1 &= \begin{pmatrix} 200 & 100 & 5 \end{pmatrix}^T m \\ s_2 &= \begin{pmatrix} 100 & -100 & 30 \end{pmatrix}^T m \\ s_3 &= \begin{pmatrix} 600 & -50 & 50 \end{pmatrix}^T m \\ s_4 &= \begin{pmatrix} 500 & 50 & 40 \end{pmatrix}^T m \\ s_5 &= \begin{pmatrix} 30 & 0 & 100 \end{pmatrix}^T m \\ s_6 &= \begin{pmatrix} 400 & 20 & 120 \end{pmatrix}^T m. \end{aligned}$$

These locations are selected for illustration purposes. The reason is that real base station locations are typically classified, which prevents the use of a live simulation scenario.

The RTT measurements are generated with a mean measurement sampling period of 1.0 s. The process noise gain matrix parameter in (24) is selected as $g = 0.001$. Process noise standard deviation for constant velocity, acceleration and hovering modes are $q_1^1 = q_2^1 = q_3^1 = 0.001\ m^2 s^{-3}$, $q_1^2 = q_2^2 = q_3^2 = 1.0\ m^2 s^{-5}$ and $q_1^3 = q_2^3 = q_3^3 = 0.01\ m^2 s^{-1}$. The measurement noise standard deviation is set to 10 m.

The mode transition probability matrix is set to

$$p_{ij} = \begin{pmatrix} 0.98 & 0.05 & 0.001 \\ 0.5 & 0.8 & 0.05 \\ 0.1 & 0.06 & 0.95 \end{pmatrix}. \qquad (58)$$

The initial covariance matrices for the three modes are chosen diagonal, with $\mathbf{P^1}(t_0|t_{-1})$ diagonal elements as $p_{11}^1 = p_{22}^1 = p_{33}^1 = 100\ m^2$, $p_{44}^1 = p_{55}^1 = p_{66}^1 = 4\ m^2/s^2$, $\mathbf{P^2}(t_0|t_{-1})$ diagonal elements as $p_{11}^2 = p_{22}^2 = p_{33}^2 = 100\ m^2$, $p_{44}^2 = p_{55}^2 = p_{66}^2 = 4\ m^2/s^2$, $p_{44}^3 = p_{55}^3 = p_{66}^3 = 1\ m^2/s^4$, and $\mathbf{P^3}(t_0|t_{-1})$ as $p_{11}^3 = p_{22}^3 = p_{33}^3 = 100\ m^2$.

Fig. 2 shows the estimated position trajectory of the UAV. The trajectory estimated by the IMM filter is very accurate, given the challenging nonlinear estimation problem. Estimated mode probabilities for the three movement models are shown in 3. It can be seen that estimated mode probabilities behave as expected and contribute to the high performance of the algorithm.

The main sources of error are the RTT measurement errors. These errors are a combination of the measurement errors in the UAV and in the base station, together with the resolution (quantization) of the RTT measurements, cf. (40). Referring to [11] and [12] that report the measurement inaccuracy for 3G, it is expected that 5G measurement errors should be at least 10 times better.

Additional potential impairments include clock offsets between measurement sites as well as signaling delays of measured information between the measuring and state estimation nodes. However, neither of these are significant. This is due to the processing of time tagged and irregularly sampled RTT measurements, meaning that signaling delays of a few milliseconds are negligible. The time tagging is typically significantly better than 1 millisecond in 5G.

The geometry of the measurement sites is another very significant factor that impacts the tracking inaccuracy. This is discussed at length in [13]. As compared to the results of [13] that combine RTT with Doppler, the accuracy is better in the present paper. The main reason is that more sites contribute to reduce the estimation errors here.

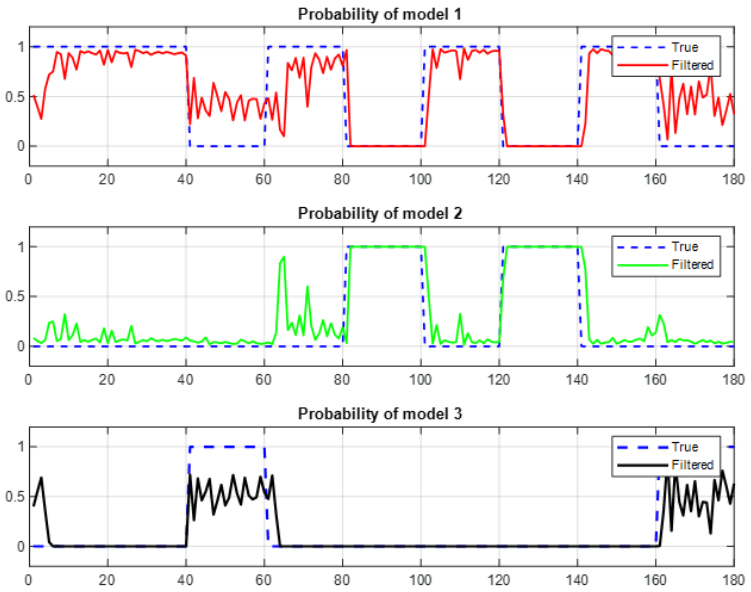

Fig. 3. Estimated mode probabilities.

IV. Conclusions

The paper considered state estimation of UAVs using an IMM algorithm in 5G cellular networks. The proposed approach employs irregularly sampled RTT measurements from multiple base stations to estimate the position, velocity and acceleration of the UAV. The IMM algorithm is designed with three movement modes, a straight line movement mode, a maneuvering flight mode and an unconventional hovering mode with nonlinear measurement equations processed by EKFs. A new restricting transition probability model was introduced. The performance of the algorithm was illustrated using a numerical example. The estimated trajectory was found to be highly accurately, exploiting all three movement modes as desired.

References

[1] K. Li, W. Ni, E. Tovar and A. Jamalipour, "Online velocity control and data capture of drones for the internet of things -an onboard deep reinforcement learning approach", IEEE Vehicular Tech. Magazine, vol. 16, no. 1, pp. 49-56, 2021.

[2] H.-L. Määattänen, "3GPP standardisation for cellular-supported UAVs", in UAV Communications for 5G and beyond, Wiley-IEEE Press, 2021. DOI: 10.1002/9781119575795

[3] S. Si-Mohammed et. al, "Supporting unmanned aerial vehicle services in 5G networks - new high-level integrating 5G with U-space", IEEE Vehicular Tech. Magazine, vol. 16, no. 1, pp. 57-65, 2021.

[4] J. Sun, G. Gui, H. Sari, H. Gacanin and F. Adachi, "Aviation data lake - using side information to enhance future air-ground vehicle networks", IEEE Vehicular Tech. Magazine, vol. 16, no. 1, pp. 40-48, 2021.

[5] "High-level regulatory framework for the U-space", European Union Aviation Safety Agency, Cologne, Germany, 2020. [Online]. Available: https://blog.masterdrones.eu/high-level-regulatory-frameworkfor-the-u-space-opinion-no-01-2020/

[6] "Unmanned Aircraft System (UAS) Traffic Management (UTM), Concept of Operations", Federal Aviation Administration, Washington, D.C, 2018. [Online]. Available: https://utm.arc.nasa.gov/docs/2018-UTMConOps-v1.0.pdf

[7] "Unmanned Aerial System (UAS) support in 3GPP", 3GPP TS 22.125, Jan, 2018. [Online]. Available: http://www.3gpp.org/DynaReport/22-series.htm

[8] "Initial view on principles for U-space architecture", SESAR Joint Undertaking, 2019. [Online]. Available: https://www.sesarju.eu/sites/default/files/documents/uspace/ SESAR

[9] Y. Bar-Shalom and X. -R. Li, *Estimation and Tracking - Principles, Techniques and Software.* Norwood, MA: Artech House, 1995.

[10] S. S. Blackman and R. Popoli, *Design and Analysis of Modern Tracking Systems.* London:UK, Artech House, 1999.

[11] J. Wennervirta and T. Wigren, "RTT positioning field performance", *IEEE Trans. Vehicular Tech.*, vol. 59, no. 7, pp. 3656-3661, 2010.

[12] T. Wigren and J. Wennervirta, "RTT positioning in WCDMA", *Proc. 5th International Conference on Wireless and Mobile Communications, ICWMC 2009*, Cannes/La Bocca, France, pp. 303-308, Aug. 23-29, 2009.

[13] T. Wigren, S. Yasini, "Passive UAV Tracking in Wireless Networks", IEEE Transactions on Aerospace and Electronic Systems, vol. 58, pp. 4101-4118. 2022.

[14] H. A. P. Blom, "A sophisticated tracking algorithm for air traffic control surveillance data", in Proc. Int. Conf. on Radar, pp. 393-398, Paris, France, May, 1984.

[15] H. A. P. Blom, "An efficient filter for abruptly changing systems", in Proc. 23rd IEEE CDC, pp. 656-658, Las Wegas, NV, USA, Dec., 1984.

[16] H. A. P. Blom and Y. Bar-Shalom, "The interacting multiple model algorithm for systems with Markovian switching coefficients", IEEE Trans. Automat. Contr., vol. 33, no. 8, pp. 780-783, 1988.

[17] M. Arulampalam, S. Maskell, N. Gordon and T. Clapp, "A Tutorial on Particle filters for online nonlinear/non-Gaussian Bayesian tracking" IEEE Trans. Signal Processing, vol. 50, no. 2, pp. 174–188, 2002.

[18] Y. Bar-Shalom, P. K. Willett, and X. Tian, Tracking and data fusion, a handbook of algorithms. YBS Publishing, 2011.